Monthly Notices
of the
ROYAL ASTRONOMICAL SOCIETY

MNRAS **471,** 4275–4285 (2017) doi:10.1093/mnras/stx1738

Explosive nucleosynthesis of ultra-stripped Type Ic supernovae: application to light trans-iron elements

Takashi Yoshida,[1]★ Yudai Suwa,[2] Hideyuki Umeda,[1] Masaru Shibata[2] and Koh Takahashi[1,3]

[1]*Department of Astronomy, Graduate School of Science, University of Tokyo, Tokyo 113-0033, Japan*
[2]*Center for Gravitational Physics, Yukawa Institute for Theoretical Physics, Kyoto University, Kyoto 606-8502, Japan*
[3]*Argelander-Institute für Astronomie, Universität Bonn, D-53121 Bonn, Germany*

Accepted 2017 July 9. Received 2017 June 8; in original form 2016 November 24

ABSTRACT

We investigate the nucleosynthesis that occurs during the two-dimensional neutrino-driven explosion of ultra-stripped Type Ic supernovae evolved from 1.45 and 1.5 $M_\odot$ CO stars. These supernovae explode with an explosion energy of $\sim 10^{50}$ erg and release ejecta of mass $\sim 0.1\ M_\odot$. The light trans-iron elements Ga–Zr are produced in the neutrino-irradiated ejecta. The abundance distribution of these elements has a large uncertainty because of the uncertainty of the electron fraction of the neutrino-irradiated ejecta. The yield of the elements will be less than $0.01\ M_\odot$. Ultra-stripped supernovae and core-collapse supernovae evolved from a light CO core could be the main sources of light trans-iron elements. They could also produce the neutron-rich nuclei ^{48}Ca. Ultra-stripped supernovae eject ~ 0.006–$0.01\ M_\odot$ of ^{56}Ni. If most of the neutrino-irradiated ejecta is proton-rich, ^{56}Ni will be produced more abundantly. The light-curves of these supernovae indicate a subluminous fast-decaying explosion with a peak magnitude of about −15 to −16. Future observations of ultra-stripped supernovae could constrain the event rate of a class of neutron star mergers.

Key words: nuclear reactions, nucleosynthesis, abundances – binaries: close – stars: massive – stars: neutron – supernovae: general.

1 INTRODUCTION

Mergers of binary compact objects such as neutron stars (NSs) and black holes (BHs) are promising sites for r-process nucleosynthesis. Detailed calculations of r-process nucleosynthesis in mergers of binary compact objects have succeeded in producing heavy r-process elements with a solar abundance pattern, taking account of general relativity and weak interactions in ejected matter (Wanajo et al. 2014; Just et al. 2015; Goriely et al. 2015).The discovery of a near-infrared excess in the short gamma-ray burst GRB 130603B (Tanvir et al. 2013) led to the suggestion that a substantial fraction of mass is likely to be ejected in NS mergers (NSMs) (Tanaka & Hotokezaka 2013; Hotokezaka et al. 2013). Furthermore, recent chemical evolution models considering proto-galactic fragments with various scales and a merger time-scale of $\sim 10^7$–10^8 yr reproduced the observed abundance ratio of the r-process elements (e.g. Komiya et al. 2014; Tsujimoto & Shigeyama 2014a; van de Voort et al. 2015; Ishimaru et al. 2015; Shen et al. 2015; Hirai et al. 2015). Because the merger rate and merging time-scale of binary compact objects still have uncertainties, it is important to constrain these values through future observations.

Ultra-stripped supernovae (SNe) are candidate generation sites of binary compact objects, especially binary NSs (Tauris et al. 2013, 2015; Moriya et al. 2017). Ultra-stripped Type Ic SNe explode weakly, and the destruction of the close binary system is expected to be suppressed (Suwa et al. 2015). The evolutionary scenarios of close binary systems of massive stars are discussed in Podsiadlowski et al. (2005). Recently, key effects during the evolution of massive-star binary systems to produce binary NSs were investigated (Tauris et al. 2017). They showed that all known close-orbit binary NS systems are consistent with ultra-stripped SNe. Close binary systems forming ultra-stripped Type Ic SNe could also result in very close systems of compact objects, so that the merger of these objects takes place within the cosmic age (Tauris et al. 2015). The fast-decaying faint Type Ic SN 2005ek (Drout et al. 2013) is considered to belong to an ultra-stripped SN (Tauris et al. 2013; Suwa et al. 2015; Moriya et al. 2017). Further observations of these SNe could constrain the merger rate and the merging period of binary compact objects. Therefore, the explosion features of ultra-stripped SNe should be clarified.It is also important to investigate the chemical composition of ultra-stripped SNe in order to constrain the light-curve and to consider their role in Galactic chemical evolution.

As single massive stars, the evolution of CO cores in the single stars forming a light Fe core could be similar to stars slightly more

★ E-mail: tyoshida@astron.s.u-tokyo.ac.jp

massive than electron-capture (EC) SN progenitors. These stars follow different evolutionary paths from more massive stars (e.g. Woosley et al. 1980; Nomoto & Hashimoto 1988; Umeda et al. 2012; Woosley & Heger 2015). It has been found that an ECSN produces some light trans-iron elements, containing nuclei with $Z \geq 31$, as well as neutron-rich intermediate nuclei (Wanajo et al. 2011). (Nucleosynthesis occurring during SN explosions having a light Fe core has been analysed recently, and it has been shown that light trans-iron elements are also produced (Wanajo et al. 2017).) If the initial mass range of these stars is not narrow, the product composition of the SNe evolving from them would contribute to the Galactic chemical evolution.

In this paper, we investigate the explosive nucleosynthesis occurring in ultra-stripped Type Ic SNe evolved from 1.45 and 1.5 $M_\odot$ CO stars. We pursue two-dimensional neutrino-radiation hydrodynamical simulations of the SN explosions of these stars for periods longer than those investigated by Suwa et al. (2015). Then, we calculate the detailed explosive nucleosynthesis of the ejecta. The paper is organized as follows. In Section 2, we describe ultra-stripped Type Ic SN models evolved from CO stars. In Section 3, we first present our calculations of nucleosynthesis. We then give the results of a detailed explosive nucleosynthesis of the SNe. We pay attention to the ^{56}Ni yield and the abundances of some neutron-rich isotopes and light trans-iron elements, including the first-peak r-process isotopes. In Section 4, we first estimate the light-curves of the ultra-stripped SNe and discuss associated observational constraints. We then discuss uncertainties in the abundance of the light trans-iron elements evaluated in this study. We also discuss the contribution of light trans-iron elements, including light r-process isotopes in ultra-stripped SNe and weak SNe evolved from single massive stars forming a light CO core, to the Solar-system composition and the Galactic chemical evolution. We conclude this study in Section 5. In Appendix A, we discuss the explosive nucleosynthesis in an ECSN. We perform a numerical simulation for the explosion of an ECSN using the same method as for the explosion of ultra-stripped SNe in order to identify the systematic differences in the explosion models.

2 ULTRA-STRIPPED TYPE IC SN MODELS

First, we perform long-term simulations of ultra-stripped SNe evolved from 1.45 and 1.5 $M_\odot$ CO stars, using the CO145 and CO15 models from Suwa et al. (2015). We follow the post-bounce phase for 1.3 s. We use the two-dimensional neutrino-radiation hydrodynamics code from Suwa et al. (2010). The basic features are the same as in Suwa et al. (2015), but equatorial symmetry is imposed in order to save computational time. Then, we follow the thermal evolution (i.e. temperature, density, radius and electron fraction) of the SN ejecta using a particle-tracer method. The properties of the explosions of the ultra-stripped SN models are summarized in Table 1. We obtain weak explosions of energy of $\sim 10^{50}$ erg and

Table 1. Properties of the ultra-stripped SN models.

Model	CO145	CO15
Progenitor mass [$M_\odot$]	1.45	1.50
Mass in the computational domain [$M_\odot$]	1.43	1.48
Final time of the calculation [s]	1.328	1.304
Explosion energy [10^{51} erg]	0.170	0.118
Ejecta mass [$M_\odot$]	0.0980	0.1121
Remnant baryon mass [$M_\odot$]	1.35	1.39
Remnant gravitational mass [$M_\odot$]	1.24	1.27

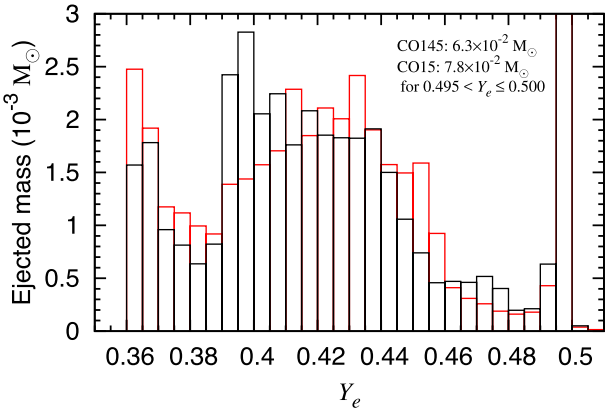

Figure 1. The ejected mass in each bin of Y_e at the initial time of the nucleosynthesis calculation. The red and black lines denote the results for the CO145 and CO15 models, respectively. The vertical axis denotes the ejected mass in units of 10^{-3} $M_\odot$ within each Y_e bin, which are of width $\Delta Y_e = 0.005$. The mass in $Y_e = 0.495$–0.50 is 6.3×10^{-2} and 7.8×10^{-2} $M_\odot$ for the CO145 and CO15 models, respectively, which is out of the scale of this figure.

small ejecta masses of $\lesssim 0.1$ $M_\odot$. We assume that the materials outside the computational domain of the hydrodynamics simulations are ejected and that they did not undergo strong explosive nucleosynthesis.

The SN ejecta have wide distributions of the electron fraction Y_e. Fig. 1 shows the ejected mass in each bin of Y_e when the nucleosynthesis calculation starts (see Section 3). The electron fraction in the ejecta is distributed as $0.360 \leq Y_e \leq 0.508$ and $0.361 \leq Y_e \leq 0.503$ in the CO145 and the CO15 model, respectively.

Here, we define two components of the SN ejecta depending on their maximum temperature. The shock-heated ejecta and neutrino-irradiated ejecta are defined as the ejecta with maximum temperature below and above 9×10^9 K, respectively. In our models, slightly less than half of the ejecta are shock-heated ejecta. These ejecta were in the outermost region of the progenitor. They are ejected before they accrete onto the proto-neutron star (PNS) and have not experienced electron capture. Hence, their electron fraction is about 0.5. The mass of the shock-heated ejecta having Y_e in the range $0.495 < Y_e \leq 0.5$ is 6.3×10^{-2} and 7.8×10^{-2} $M_\odot$ for the CO145 and the CO15 model, respectively. In the ejecta, the mass of the fluid components for which the temperature increases above 5×10^9 K is 1.1×10^{-2} and 5.6×10^{-3} $M_\odot$ for the CO145 and the CO15 model. The main product of these components is ^{56}Ni, generated through explosive Si-burning. The other component (with the maximum temperature lower than 5×10^9 K) contains O, Ne and other intermediate elements.

The neutrino-irradiated ejecta experience a high-temperature state and have different electron fractions depending on the neutrino irradiation. The electron fraction of the ejecta is distributed mainly in the range between 0.36 and 0.45. The mass of the ejecta with $Y_e > 0.45$ is smaller than that of more neutron-rich ejecta. Proton-rich materials are hardly ejected.

Because the Y_e distributions depend on numerical methods and there have been no studies investigating nucleosynthesis on ultra-stripped SNe, we also perform a simulation of an ECSN in order to compare our results with those of Wanajo et al. (2011). The nucleosynthesis results for the ECSN are given in Appendix A.

We note that Müller (2016) discussed the condition of ECSN-like explosions using the density profile of SN progenitors and the

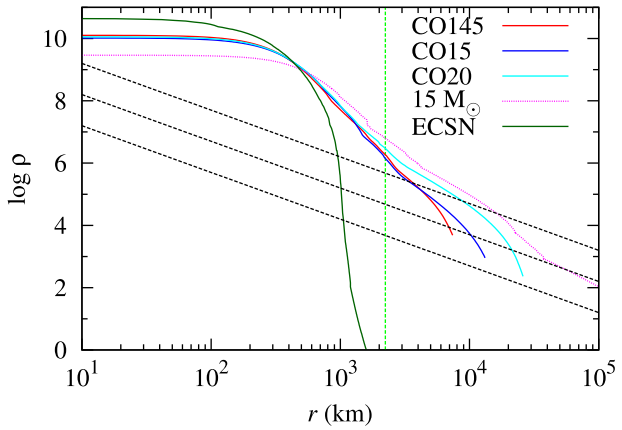

Figure 2. The density profiles of the CO145 (red line), CO15 (blue line) and CO20 (cyan line) models and of the 15 $M_\odot$ (pink dashed line) and ECSN progenitor (green line) models for comparison. The top, middle and bottom dashed lines denote the density that results in an accretion rate of 0.05, 5×10^{-3}, and 5×10^{-4} $M_\odot\,s^{-1}$, respectively (Müller 2016). The vertical dashed line denotes 2230 km. See text for details.

critical mass accretion rate. In his discussion, the density needs to decrease to

$$\rho \lesssim \frac{1}{8}\sqrt{\frac{3}{Gm}}\dot{M}_{\rm crit} r^{-3/2}, \quad (1)$$

where G is the gravitational constant, m is the core mass of the progenitor, $\dot{M}_{\rm crit}$ is the critical mass accretion rate and r is the radius. This condition should be satisfied for a radius of $r < 2230$ km in order to obtain ECSN-like explosion dynamics. A critical mass accretion rate of $\dot{M}_{\rm crit} \sim 0.07$ $M_\odot\,s^{-1}$ is expected for ECSN-like progenitors. Here we apply this condition to the ultra-stripped SN models CO145 and CO15. Fig. 2 shows the density profiles of the CO145, CO15 and CO20 (Suwa et al. 2015) models, and of 15 $M_\odot$ (Yoshida et al. 2016) and ECSN models (Nomoto 1987) for comparison. It also shows the density profiles of equation (1) using $m = 1.4$ $M_\odot$ and $\dot{M}_{\rm crit} = 0.05$, 5×10^{-3}, and 5×10^{-4} $M_\odot\,s^{-1}$ in accordance with Müller (2016). The CO145 and CO15 models seem to be marginal cases for obtaining ECSN-like explosions. The density profiles of $r \gtrsim 3000$ km show a steeper decrease than the s10.09 and s11.2 models in Müller (2016).

3 EXPLOSIVE NUCLEOSYNTHESIS IN ULTRA-STRIPPED SUPERNOVAE

We calculate the explosive nucleosynthesis in the SN ejecta of the CO145 and CO15 models using the thermal history of 9968 and 8875 traced fluid particles, respectively, which have positive energy and positive radial velocity. We use the nuclear reaction network consisting of 1651 nuclear species listed in Table 2.We determine the nuclear species to cover the nuclear flow in the fluid particles having the smallest and largest Y_e values using the reaction network of 5406 nuclear species (Fujibayashi et al. 2015).

We select three initial conditions for the particles, depending on the maximum temperature. For particles for which the temperature exceeds 9×10^9 K, we calculate the nucleosynthesis from the time when the temperature decreases to 9×10^9 K. The initial composition is set as the composition in nuclear statistical equilibrium (NSE), with the Y_e value calculated in the hydrodynamical simulation. For particles with a maximum temperature of (7–9) $\times 10^9$ K, we start the calculation from the time at the maximum temperature

Table 2. The 1651 nuclear species adopted in the nuclear reaction network. The isomeric state of ^{26}Al is taken into account.

Element	*A*	Element	*A*	Element	*A*
n	1	Ca	33–62	Zr	76–120
H	1–3	Sc	36–64	Nb	80–124
He	3, 4, 6	Ti	37–68	Mo	81–127
Li	6–9	V	40–71	Tc	84–128
Be	7, 9–12	Cr	42–75	Ru	85–129
B	8, 10–14	Mn	44–77	Rh	88–130
C	9–18	Fe	45–79	Pd	89–132
N	12–21	Co	47–81	Ag	92–133
O	13–22	Ni	48–83	Cd	94–135
F	17–26	Cu	51–86	In	97–136
Ne	17–29	Zn	52–88	Sn	99–137
Na	18–32	Ga	56–92	Sb	100–138
Mg	19–36	Ge	58–95	Te	114–139
Al	21–40	As	61–98	I	121–141
Si	22–43	Se	62–100	Xe	122–142
P	23–45	Br	66–102	Cs	125–143
S	24–49	Kr	67–107	Ba	126–143
Cl	28–51	Rb	70–110	La	131–143
Ar	29–55	Sr	71–113	Ce	132–143
K	32–58	Y	74–116		

with the NSE initial composition. For other particles, we calculate the nucleosynthesis from the initial time of the hydrodynamical simulation with the composition in the O/Ne layer. The nucleosynthesis calculation is continued until the temperature decreases to 10^7 K. At the time of the termination of the hydrodynamical simulation, we determine the radial motion and thermal evolution assuming adiabatic expansion with a constant velocity. We take into account the ν-process in a simple manner. The neutrino luminosity is assumed to decrease exponentially with a time-scale of $\tau_\nu = 3$ s (Woosley et al. 1990). The total neutrino energy radiated is set to be 3×10^{53} erg and is equipartitioned among each flavour. The neutrino energy distribution obeys the Fermi–Dirac distribution with temperature $(T_{\nu_e}, T_{\bar{\nu}_e}, T_{\nu_{\mu,\tau}, \bar{\nu}_{\mu,\tau}}) = (4\ \text{MeV}, 4\ \text{MeV}, 6\ \text{MeV})$ and zero chemical potentials (Yoshida et al. 2008). Although the adopted $\nu_{\mu,\tau}$ temperature is larger than that obtained from recent spectral transport (e.g. Fischer et al. 2010; Müller 2012), this large value has a negligible effect on the abundance distribution of the ejecta.

Fig. 3 shows the mass fraction distribution of isotopes in the SN ejecta of the CO145 and CO15 models. The yields of some elements and isotopes ejected in the CO145 and CO15 models are listed in Table 3. The general features are the same for the CO145 and CO15 models. Most of isotopes with mass $A \lesssim 90$ are produced with the mass fraction above 10^{-3}. Elements with $90 \lesssim A \lesssim 130$ are also produced, but their mass fractions decrease with mass number.

Most of the C, O, and intermediate nuclei with $A \lesssim 40$ are mainly unburned or synthesized through explosive O-burning. Light iron-peak elements, Ti, V and Cr, are produced in neutron-rich ($Y_e \lesssim 0.40$) material. Mn and Fe are produced through explosive Si-burning. The ^{56}Ni yield is 9.73×10^{-3} and 5.72×10^{-3} $M_\odot$ in the CO145 and the CO15 model, respectively. These values are smaller than the expectations in Suwa et al. (2015). This is because some of the materials that experienced a temperature higher than 5×10^9 K are neutrino-irradiated ejecta. They become neutron-rich and are synthesized to form lighter and heavier elements. Heavy neutron-rich isotopes of $A \sim 60$–90 are also produced in the neutrino-irradiated ejecta containing neutron-rich material. The first-peak r-process isotopes such as $^{72-74,76}$Ge, ^{75}As, ^{77,78,80,82}Se, ^{81}Br, ^{83,84,86}Kr, ^{85,87}Rb and ^{88}Sr (table 1 in Sneden et al. 2008) are

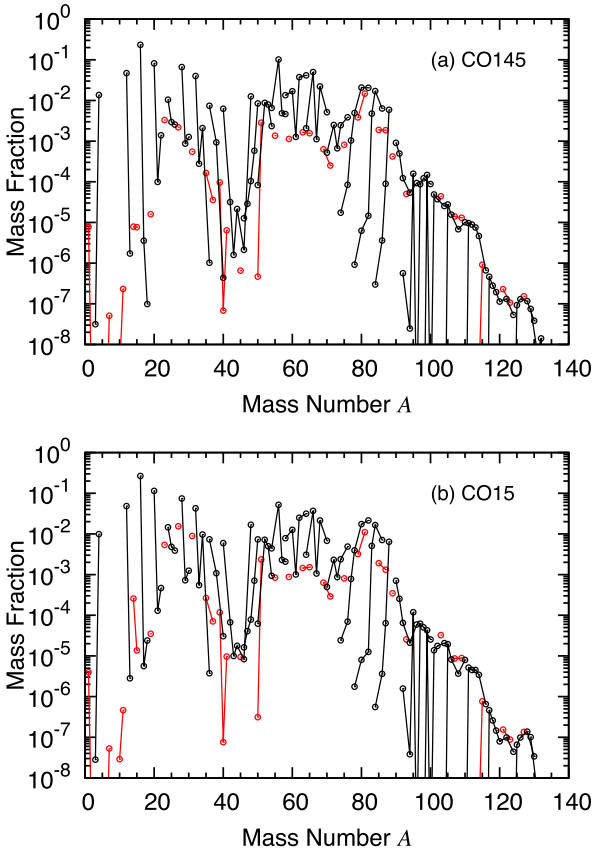

Figure 3. Mass fraction distribution of isotopes in the ejecta of ultra-stripped Type Ic SNe. Panels (a) and (b) denote the CO145 and the CO15 model, respectively. The red and black lines correspond to odd-Z and even-Z isotopes.

included. They are produced in nuclear quasi-equilibrium (Meyer et al. 1998; Wanajo et al. 2011). On the other hand, most ^{56}Ni is produced in the shock-heated ejecta.

We now consider the contribution to the Solar system composition. Fig. 4 shows the elemental abundance ratios to the Solar system composition. The elemental abundance ratio means that the ratio of the abundance in the SN ejecta to the normalized solar abundance in Asplund et al. (2009) for each element. Elements As–Sr have high abundance ratios, namely more than 10 per cent of the highest abundance ratio. The element with the highest abundance ratio is Br. The ratios of the heavier elements Y–Rh are lower than for the above elements, but the ratios are still higher than for other elements. Se, Br and Kr are produced mainly in the ejecta of $Y_e \sim 0.36$–0.43. On the other hand, Sr, Y and Zr are produced in $Y_e \sim 0.36$–0.38 as well as in 0.42–0.46. Because the ejecta mass of material with $Y_e \gtrsim 0.44$ is small, the contribution of Sr–Zr is smaller than that of Se–Kr. The light trans-iron elements produced in ultra-stripped SNe may contribute to the Solar system abundance and the Galactic chemical evolution. Further details of the dependence of the synthesis of trans-iron elements on Y_e will be given in Section 4.2.

Fig. 5 shows the isotopic abundance ratios to the Solar system composition in the CO145 and CO15 models. The isotopic abundances in the Solar system composition are adopted from Lodders et al. (2009). The yields of some isotopes are also listed in Table 3. The isotopes of $A \sim 70$–100 have high abundance ratios. We also see high ratios of ^{48}Ca. The obtained ratio of ^{48}Ca is similar to that for ECSNe. Although it has been shown that ^{48}Ca is produced in low-entropy neutron-rich ($Y_e \sim 0.42$) expansions (Meyer et al. 1996), the origin of ^{48}Ca has not been clarified. The possibility of the production in neutron-rich ejecta of SNe Ia was proposed in Woosley (1997). ECSNe have been suggested as a possible site of ^{48}Ca (Wanajo et al. 2013a). Ultra-stripped SNe and core-collapse SNe evolved from light CO cores are possible sites of ^{48}Ca.

4 DISCUSSION

4.1 Light-curves of ultra-stripped SNe

We derive light-curve models of ultra-stripped SNe for the CO145 and CO15 models using the analytic solution shown in Arnett (1982). The energy generation rates of ^{56}Ni and ^{56}Co are adopted from Nadyozhin (1994). We use the deposition factor of ^{56}Co as $D_{\rm Co} = 0.968D(\tau_\gamma) + 0.032D(355\tau_\gamma)$, where τ_γ is the optical depth of gamma-rays, to take into account both the gamma-ray energy release and the positron kinetic energy release (Nadyozhin 1994; Colgate et al. 1997). We adopt $\kappa = 0.1\,{\rm cm^2\,g^{-1}}$ for the opacity of the SN ejecta. We include the approximate effect of gamma-ray leakage using the deposition function, as shown in Arnett (1982) (see also Colgate et al. 1980). The corresponding gamma-ray opacity is $\kappa_\gamma = 0.03\,{\rm cm^2\,g^{-1}}$. We consider the energy release by the radioactive decay of intermediate and heavy elements. The fractions of the energy deposition by gamma-rays and positrons from their radioactive decay are not known. Hence, we assume the energy deposition fractions by gamma-rays and positrons as 0.5 for simplicity.

Fig. 6 shows the light-curves of these SNe. For comparison, we also show the light-curve of the fast-decaying Type Ic SN 2005ek, for which the ejecta mass and ^{56}Ni mass were estimated as 0.1 $M_\odot$ and 0.03 $M_\odot$ by Drout et al. (2013). The peak absolute magnitude of our models is -15.5 to -16. We also vary the yield ranges for ^{56}Ni and other radioactive isotopes between twice and a half of the values obtained numerically. The range of the peak absolute magnitude varies in the range -14.8 to -16.5. When the yields of ^{56}Ni and other radioactive isotopes are twice in the CO145 model, the light-curve reproduces that of SN 2005ek.

The energy release of the radioactive decay of iron-peak elements other than ^{56}Ni and ^{56}Co partly contributes to the optical emission. In the CO145 model, the radioactive decay of these elements makes a contribution for 1 d after the collapse. The fraction of the luminosity from these elements is 27 per cent at the peak luminosity. In the CO15 model, however, the radioactive decay from these elements makes a contribution for 4 d. If the contribution from these elements

Table 3. Yields of various elements and isotopes in units of 10^{-3} $M_\odot$.

Element	CO145	CO15	Element	CO145	CO15	Isotope	CO145	CO15	Isotope	CO145	CO15
C	4.60	5.41	Si	6.71	8.56	^{48}Ca	1.24	1.88	^{53}Mn	0.00200	0.00203
O	22.9	29.7	S	4.14	5.91	^{50}Ti	0.825	0.821	^{56}Ni	9.73	5.72
Ne	8.12	12.9	Ca	4.14	5.91	^{26}Al	0.214	0.211	^{60}Fe	0.528	0.343
Mg	1.56	2.61	$Z \geq 31$	11.6	12.4	^{41}Ca	0.000593	0.000798			

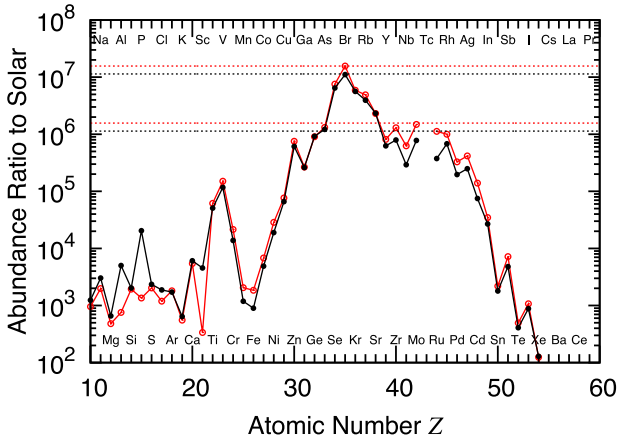

Figure 4. Abundance ratios of elements in the ejecta of ultra-stripped Type Ic SNe to the solar abundance. The red and black lines denote the ratios of the CO145 and CO15 models, respectively. The dashed lines denote the maximum ratios and the ratios of the 10 per cent of the maximum ratios.

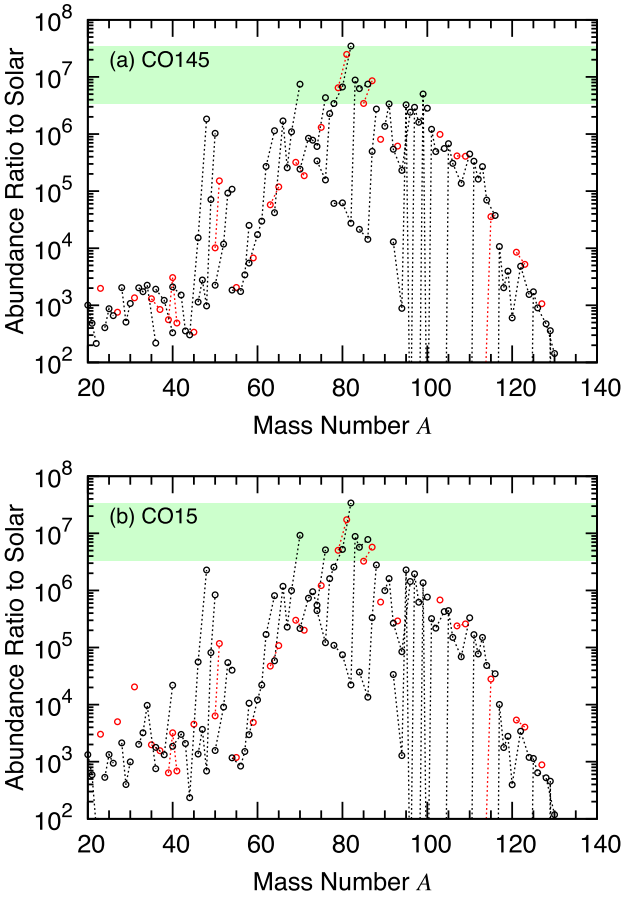

Figure 5. Abundance ratios of isotopes in the ejecta of the (a) CO145 and (b) CO15 model to the solar abundance. The red and black lines correspond to odd-Z and even-Z nuclei. The green-hatched region denotes the range of the abundance ratio between the maximum and one-tenth of that.

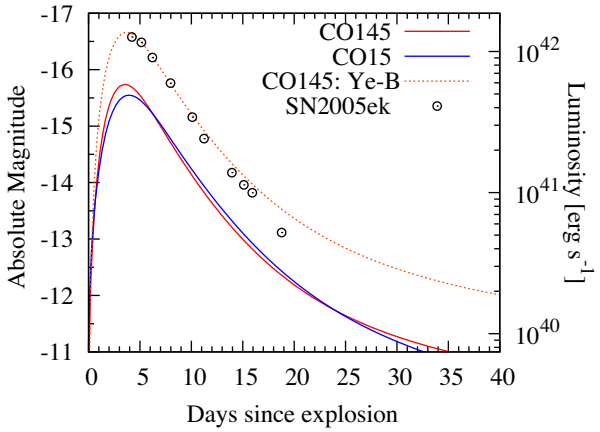

Figure 6. Light-curves of the ultra-stripped Type Ic SNe. The red and blue curves denote the CO145 and CO15 models, respectively. The circles denote the light-curve of SN 2005ek. The orange dashed line denotes the CO145 Ye-B model (see Section 4.2).

is ignored, the peak luminosity is approximately halved. The main energy source other than ^{56}Ni and ^{56}Co is ^{57}Ni and ^{66}Cu for the CO145 and the CO15 model, respectively. The decay time of the luminosity from these elements is about 4 and 8 d in the CO145 and the CO15 model, respectively. The difference of the contribution from these elements is mainly the result of the difference in the ^{56}Ni yield.

Recently, a variety of fast-decaying SNe have been found in survey programs for transient objects. Subluminous SNe have also been observed as Types Ia and Ib/c SNe (e.g. Foley et al. 2013; Drout et al. 2014). Some subluminous fast-decaying SNe could be ultra-stripped SNe. These observed SNe showed spectral features different from those of normal Types Ia and Ib/c SNe. The ejecta of the ultra-stripped SNe in our models indicate a higher abundance ratio of intermediate elements to oxygen compared with the case for more massive CO cores. These compositional differences could give distinctive spectral features. The identification of ultra-stripped SNe from Type I SNe is important for the evaluation of the ultra-stripped SN rate. Future observations of ultra-stripped SNe could constrain the rates of ultra-stripped SNe.

We note, as pointed out in Suwa et al. (2015), that it is safe to consider that our results give a lower limit of the explosion energy of an ultra-stripped SN. In the case of a stronger explosion of an ultra-stripped SN, the ejected ^{56}Ni mass could be larger. If so, ultra-stripped SNe could be observed as fast-decaying SNe such as the Type Ic SN 2005ek. We also note that the ^{56}Ni mass would be underestimated because of the missing proton-rich component in the neutrino-irradiated ejecta. This will be discussed in Section 4.2.

4.2 Uncertainties of the yield of light trans-iron elements in ultra-stripped SN models

We obtained light trans-iron elements in the ultra-stripped SN models. However, the production efficiency of the elements depends on the Y_e distribution of the SN ejecta, which in turn depends on the detailed treatment of neutrino transport. Indeed, Müller (2016) showed that an approximate treatment of neutrino transport introduces a broader Y_e distribution than in a more stringent model including sophisticated microphysics. On the other hand, an update of the code can even lead to a smaller Y_e distribution. For instance, an ECSN simulation performed by the Garching group with an updated code showed a smaller minimum value of Y_e (0.34) than the previous result (0.404; Wanajo et al. 2011) (Janka 2016, private

communication[1]). Therefore, it appears that the Y_e distribution is sensitive to the detailed treatment of the microphysics, including the neutrino transfer method. In order to assess the uncertainties originating from the difference in the codes, we performed numerical simulations of an ECSN with our code used in the simulations of the ultra-stripped SNe and carried out a simulation of the explosive nucleosynthesis. We compared the ECSN yield with the result in Wanajo et al. (2011) and found that more neutron-rich material is ejected in our model (see Appendix A).

In order to study the uncertainties in the yield of trans-iron elements more systematically, we here consider two methods to modify the Y_e distributions of the CO145 model. In the first method, we consider three cases of the Y_e distributions by increasing the minimum Y_e value. We refer to the three models as the Ye040, Ye042 and Ye044 models. Ye*XXX* indicates that the minimum Y_e value in the corresponding model, $Y_{e,min}$, is *X.XX*. We modify the Y_e values of the tracer particles according to

$$Y_{e,mod} = \frac{0.50 - Y_{e,min}}{0.14}(Y_e - 0.36) + Y_{e,min} \quad (2)$$

for $Y_e \leq 0.5$ in each model.

In the second method, we consider two cases of the Y_e distribution based on Wanajo et al. (2011) and Buras et al. (2006), in which the Y_e distributions of ECSN and 15 $M_\odot$ CCSN models are considered, respectively. In the ECSN model, the Y_e value of the ejecta ranges between 0.404 and 0.54 (fig. 2 in Wanajo et al. 2011). The peak of the ejecta mass is at $Y_e \sim 0.48$. In the 15 $M_\odot$ CCSN model, the Y_e value of the ejecta ranges between 0.470 and 0.555 (fig. 41 in Buras et al. 2006). The ejecta mass in each Y_e-bin with $\Delta Y_e = 0.005$ varies in the range of 10^{-4}–0.01 $M_\odot$, and the peak is located at $Y_e \sim 0.50$. We refer to the former and the latter models as the Ye-W and the Ye-B model, respectively. We construct two modified Y_e models having similar Y_e distributions to these two models, as follows. First, we pick up tracer particles in the neutrino-irradiated ejecta and calculate the mass fraction to the total mass of the neutrino-irradiated ejecta for each particle. Next, we set the particles in incremental order of Y_e. We calculate the cumulative mass fraction c_M as a function of Y_e for each particle. Then, we set the modified Y_e values using the following equations:

$$Y_{e,mod} = \begin{cases} 0.48 + 0.04\log_{10}(1.73c_M + 0.01) & \text{for } c_M \leq 4/7 \\ 0.48 - 0.06\log_{10}(2.31(1 - c_M) + 0.01) & \text{for } c_M \geq 4/7 \end{cases} \quad (3)$$

for the Ye-W model, and

$$Y_{e,mod} = \begin{cases} 0.5 + 0.015\log_{10}(2.64c_M + 0.01) & \text{for } c_M \leq 0.375 \\ 0.5 - 0.025\log_{10}(1.58(1 - c_M) + 0.01) & \text{for } c_M \geq 0.375 \end{cases} \quad (4)$$

for the Ye-B model. The obtained Y_e distribution is shown in Fig. 7. The mass fraction of the particles of $Y_e > 0.5$ in the neutrino-irradiated ejecta is 0.09 and 0.63 for the Ye-W and the Ye-B model, respectively. We do not modify the Y_e values of the shock-heated ejecta.

First, we present the result of the Ye040, Ye042 and Ye044 models. Fig. 8 shows the elemental abundance ratios to the Solar system

[1] See also http://www2.yukawa.kyoto-u.ac.jp/~npcsm/conference/slides/01Tue/Janka.pdf.

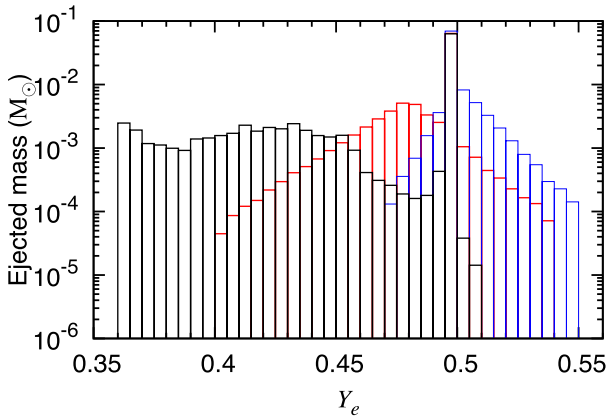

Figure 7. As Fig. 1, but for the modified Y_e cases of the CO145 model. The red, blue and black lines denote CO145-Ye-W, CO145-Ye-B and the unmodified CO145 model, respectively.

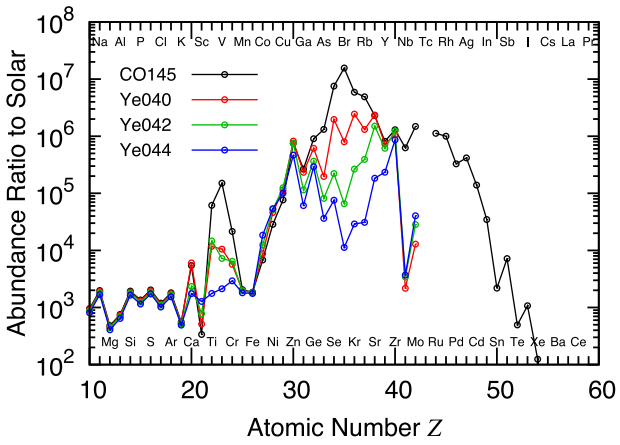

Figure 8. Abundance ratios of elements in the ejecta of ultra-stripped SN models to the solar abundance. The black, red, green and blue lines denote the ratios of the CO145, Ye040, Ye042 and Ye044 models, respectively.

composition. Light trans-iron elements are produced in the three models. However, the dependence of the abundance ratios on the Y_e distribution varies among the elements. The abundance ratios of Ge and Zr depend weakly on the Y_e distribution in these Y_e modifications. By contrast, the abundance ratios of the elements around the first r-peak such as Se and Br depend strongly on the Y_e distribution. In the Ye040 model, we find a moderate variation in the abundance ratios among Ga–Zr. The Ye044 model shows a decrease in the abundance ratios for Ga and As–Rb. We also see a strong Y_e dependence in Ti–Cr.

Fig. 9 shows the isotopic abundance ratios to the Solar system composition for Ye040 and Ye044. There is a clear difference in the isotopic abundance ratios for the two models. The distribution of the Ye040 model indicates high abundance ratios for neutron-rich nuclei for most Fe-peak elements and trans-iron elements up to Sr. There is a decrease in the abundance ratios of neutron-rich isotopes for Zr and Mo. In the Ye044 model, on the other hand, a high abundance ratio of neutron-rich nuclei is limited in iron-peak elements up to Ni. For elements heavier than Zn, except for Sr, p-nuclei rather than neutron-rich nuclei indicate high abundance ratios. The production of light p-nuclei in such slight neutron-rich materials was found by Hoffman et al. (1996). Thus, the isotopic

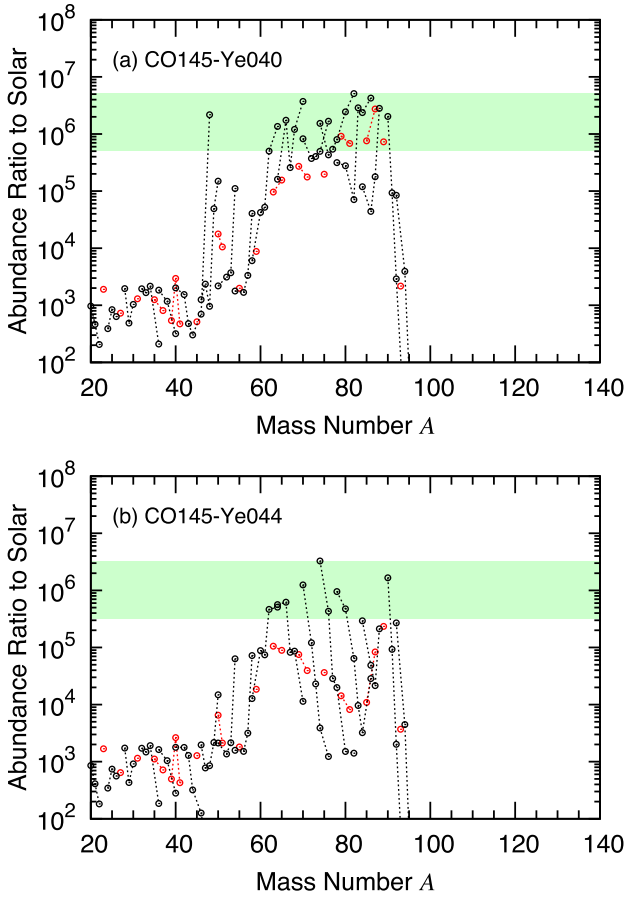

Figure 9. As Fig. 5, but for the (a) Ye040 model and (b) Ye044 model.

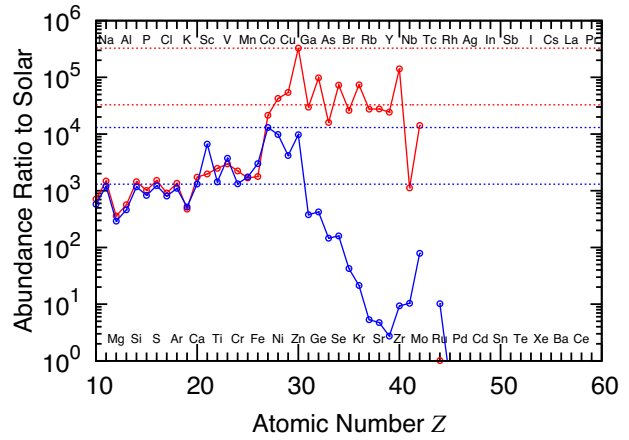

Figure 10. As Fig. 8, but for the Ye-W (red line) and Ye-B (blue line) models.

abundance distribution also depends on the Y_e distribution of the SN ejecta.

Next, we present the abundance distributions of the Ye-W and Ye-B models. Fig. 10 shows the elemental abundance ratios to the Solar system composition for the two models. The isotopic abundance ratios to the Solar system composition are shown in Fig. B1 in Appendix B. High abundance ratios of the light trans-iron elements are obtained in the Ye-W model. Zr shows the highest abundance ratio among the elements. On the other hand, a high abundance ratio is shown in the iron-peak elements with $Z \sim 22$–30 in the Ye-B model. The production of the light trans-iron elements in the Ye-B model does not contribute to the Solar system composition.

We note that the ^{56}Ni yield is 2.9×10^{-2} M$_\odot$ in the Ye-B model. This yield is three time as large as that in the original CO145 model. The light-curve for the Ye-B model is shown in Fig. 6. The maximum absolute magnitude is close to that of SN 2005ek. Note that a large amount of Sc is produced in the Ye-B model. Most of the Sc is produced in the proton-rich neutrino-irradiated ejecta. This production process of Sc was obtained in Pruet et al. (2005) and Fröhlich et al. (2006).

In order to understand the obtained abundance features, we investigate the Y_e dependence of the elemental mass fractions and abundant isotopes for even elements in the ejecta of the CO145 model. The Ge mass fraction distribution on Y_e has two peaks, at $Y_e \sim 0.39$–0.40 and $Y_e \sim 0.46$. The former peak is about five times larger than the latter. Sr and Zr also have two peaks in their mass fraction distribution on Y_e. One is at $Y_e \sim 0.36$. The other is at $Y_e \sim 0.43$–0.45 and $\sim$0.46 for Sr and Zr, respectively. We find that the mass fraction distributions of Ga, Ge and Sr–Zr have a similar Y_e dependence and that these elements are produced in the ejecta of $Y_e \gtrsim 0.44$. Thus, the yields of these elements in the SN ejecta depend only weakly on the uncertainty of the Y_e distribution.

The mass fractions of Se and Kr are, however, larger in the range of $Y_e \lesssim 0.41$ and 0.43, respectively. The mass fraction distribution of Mo has a peak at $Y_e \sim 0.36$. Although Mo is also produced in the ejecta of $Y_e \sim 0.47$, the mass fraction in the ejecta is smaller than the neutron-rich ejecta by more than two orders of magnitude. Thus, Se–Rb, Nb and Mo have a strong dependence on the Y_e distribution.

The abundant isotopes also depend on Y_e. In the ejecta of $0.36 \leq Y_e \leq 0.40$, the isotopes for which the mass fraction X is larger than 0.01 are ^{72}Ge, ^{76}Ge, ^{78,80,82}Se, ^{79,81}Br and ^{83,84}Kr. The mass fractions of the isotopes ^{74}Se, ^{75}As, ^{77}Se, and ^{85,87}Rb exceed 5×10^{-3}. In the less neutron-rich ejecta of $0.40 < Y_e \leq 0.44$, the abundant isotopes ($X > 0.01$) are ^{78,80,82}Se, ^{84,86}Kr and ^{88}Sr. The secondary abundant isotopes ($X > 5 \times 10^{-3}$) are ^{74,76}Ge, ^{83}Kr and ^{87}Rb. In the ejecta of $0.44 < Y_e \leq 0.48$, the isotopes with $X > 5 \times 10^{-3}$ are ^{70,72}Ge, ^{88}Sr and ^{90}Zr. The isotopes in the first r-process peak, ^{76}Ge, ^{75}As, ^{80}Se, ^{82}Se and ^{81}Br, are produced mainly in the ejecta of $Y_e \sim 0.36$–0.42. A similar dependence of the abundantly produced isotopes on Y_e has been found for the nucleosynthesis of an ECSN (Wanajo et al. 2011).

The yield of the light trans-iron elements also depends on the Y_e distribution. The yields in the Ye040, Ye042 and Ye044 models are 4.2×10^{-3}, 1.4×10^{-3} and 6.5×10^{-4} M$_\odot$, respectively. They decrease with the increasing minimum Y_e value in the Y_e distributions. The yields of the light trans-iron elements in the Ye-W and Ye-B models are 3.0×10^{-4} M$_\odot$ and 1.1×10^{-6} M$_\odot$, respectively. The former model has a minimum Y_e value of 0.40, but the amount of $Y_e \leq 0.44$ ejecta is only 6 per cent of the total ejecta. The latter model shows the largest minimum Y_e value among the modified Y_e models. This is a result of the Y_e dependence of the yield. We investigate the relation of the mass fractions of the light trans-iron elements with the Y_e value in the ejecta. In ejecta with $Y_e \lesssim 0.40$, the mass fraction is roughly 0.7. It decreases with increasing Y_e. It is less than 0.5, 0.2 and 0.1 for the ejecta of $Y_e \gtrsim 0.41$, 0.43 and 0.45, respectively, in the CO145 model. The above dependence is commonly seen in the modified Y_e models. We also note that the total mass of the neutrino-irradiated ejecta depends on the treatment of the neutrino transport in explosion models. This effect will increase the uncertainty in the yield of the light trans-iron elements.

We consider that the trans-iron elements up to Zr are produced in ultra-stripped SNe. However, their elemental and isotopic abundances and the total yield depend on the Y_e distribution and the minimum Y_e value in the SN ejecta. In this study, the yield of light trans-iron elements is between 1×10^{-6} and 0.01 $M_\odot$.

The ^{48}Ca yield also depends on the uncertainty of the Y_e distribution in the SN ejecta. The ^{48}Ca yield is 1.5×10^{-3}, 1.8×10^{-4} and 1.0×10^{-8} $M_\odot$ in the Ye040, Ye042 and Ye044 models, respectively. We also obtain a ^{48}Ca yield of 8.1×10^{-5} $M_\odot$ in the Ye-W model. It has been found that ^{48}Ca is produced in low-entropy neutron-rich ($Y_e \sim 0.42$) material (Meyer et al. 1996). The very small ^{48}Ca yield is a result of the lack of a production site. Ultra-stripped SNe would be a production site of ^{48}Ca. Reducing the uncertainty in the Y_e distribution will also constrain the ^{48}Ca yield in ultra-stripped SNe.

4.3 Contribution of the first-peak r-process isotopes to the Galactic chemical evolution

We obtained a light trans-iron elemental yield of $\sim 1 \times 10^{-6}$ to 0.01 $M_\odot$ containing the first-peak r-process isotopes for the CO145 and CO15 models, taking into account the assumed uncertainty in the electron fraction distributions. Here, we discuss the contributions of ultra-stripped SNe to the Solar system composition and the Galactic chemical evolution for the r-process isotopes. We consider $^{72-74,76}$Ge, ^{75}As, ^{77,78,80,82}Se, ^{81}Br, ^{83,84,86}Kr, ^{85,87}Rb and ^{88}Sr as the first-peak r-process isotopes (Sneden et al. 2008).

Possible sites of heavy r-process elements were investigated using the abundance of the short-lived isotope ^{244}Pu in interstellar particles found on Earth's deep sea-floor by Hotokezaka et al. (2015). These authors found that the production of more than 0.001 $M_\odot$ of r-process elements by NSMs with a NSM rate lower than 90 Myr^{-1} can explain the production of the r-process elements in the Galaxy. The near-infrared excess of GRB 130603B indicates that the ejecta mass of this NSM should be larger than 0.02 $M_\odot$ (Hotokezaka et al. 2013). Recent numerical simulations of NSMs (Wanajo et al. 2014; Sekiguchi et al. 2015, 2016) and the observations of heavy element ratios in metal-poor stars in dwarf spheroidal galaxies (Tsujimoto & Shigeyama 2014a) have suggested a mass of $\sim$0.01 $M_\odot$ for NSM ejecta. The abundance pattern of r-process isotopes shows that the yield ratio of the first-peak r-process isotopes to the heavier ones is about four (Sneden et al. 2008). Therefore, an additional $\sim$0.04 $M_\odot$ of first-peak r-process isotopes from an ultra-stripped SN is necessary to produce the solar r-process abundance pattern. In this study, the yield of the first-peak r-process isotopes in an ultra-stripped SN is less than 0.01 $M_\odot$. If we assume that all binary neutron stars, which merge within the cosmological age, are formed after the explosions of ultra-stripped SNe, this yield could explain 25 per cent of the solar r-process abundance at most. We therefore need other sources for producing the first-peak r-process isotopes. We will discuss ECSNe and weak SNe from light Fe cores as other candidates for the sources of light r-process isotopes in Section 4.4.

Although NSMs are now the most promising site for heavy r-process elements in very metal-poor stars, the origin of the first-peak r-process isotopes is still under debate. Tsujimoto & Shigeyama (2014b) proposed that the first-peak r-process isotopes were produced in core-collapse SNe rather than in NSMs from the observed anti-correlation of the abundance ratios of Eu/Fe and Sr/Fe. However, some outlier stars with an enrichment of Sr/Fe compared with the anti-correlation and large Eu/Fe ratio were observed. These authors considered that these stars provide evidence for the enrichment of both light and heavy r-process isotopes by NSMs. Here, we showed the possibility that ultra-stripped SNe occurred before NSMs also produce the first-peak r-process isotopes. Although there is uncertainty in the abundance distribution of the r-process isotopes, ultra-stripped SNe could be a site for light r-process isotopes of such very metal-poor stars.

4.4 A small CO core as a progenitor of a weak SN evolved from a single massive star

A star having a CO core slightly heavier than the progenitor of an ECSN ignites Ne in off-centre regions (Woosley et al. 1980; Nomoto & Hashimoto 1988; Umeda et al. 2012; Woosley & Heger 2015). The evolutionary path of such a star after the C-burning is similar to that of the progenitors of ultra-stripped SNe. Therefore, the SN explosion for it is expected to be weak, as for an ultra-stripped SN, and the SN would also produce the first-peak r-process isotopes. Here, we discuss the production of the first-peak r-process isotopes in weak SNe evolved from single massive stars having a CO core slightly heavier than an ECSN progenitor.

We discuss the initial mass range of weak SNe having a light CO core, assuming that the yield of the first-peak r-process isotopes of a weak SN is M_R $M_\odot$. We roughly estimate the total mass of the first peak r-process isotopes in the Galaxy as $\sim 2 \times 10^4$ $M_\odot$ from the heavy r-element mass in the Galaxy (Hotokezaka et al. 2015) and the r-process abundance distribution (Sneden et al. 2008). Considering the above and the age of the Universe ($\sim 1.4 \times 10^{10}$ yr), we deduce the rate of weak SNe as $\sim (7 \times 10^5 M_R)^{-1}$ yr^{-1}. If the SN rate in the Galaxy is $\sim$0.01 yr^{-1}, the ratio of weak SNe to all SNe is $R_{wk} \sim (7 \times 10^3 M_R)^{-1}$. In this case, the yield of the first-peak r-process isotopes is $\sim 1.4 \times 10^{-4} R_{wk}^{-1}$ $M_\odot$ if all first-peak r-process isotopes are produced by weak SNe. If we assume the Salpeter initial mass function, $N(M) \propto M^{-2.35}$, the mass range of weak SN progenitors is in the range from M_L to $(1 - R_{wk})^{-1/1.35} M_L$, where M_L is the lowest initial mass of weak SN progenitors. If the lower limit is 10 $M_\odot$ and the yield of the first-peak r-process isotopes is 0.01, 10^{-3} and 5×10^{-4} $M_\odot$, the upper limit of the progenitor mass of weak SNe is $\sim$10.1, 11.2 and 12.8 $M_\odot$. This rough estimate indicates that the initial mass range of weak SNe like ultra-stripped SNe could be very narrow, but it also could be one to a few $M_\odot$.

Recently, the advanced evolution of single stars covering the progenitors of ECSNe and core-collapse SNe has been investigated, and the fates of these stars discussed (Umeda et al. 2012; Woosley & Heger 2015). The initial mass range of the stars that experience off-centre O/Ne ignition is about 1 $M_\odot$, although the lower end of the mass is different in these studies. Hence, the mass range does not change significantly, even if one considers uncertainties by different convective treatments in stellar evolution models or the effect of stellar rotation. In this case, the production of 10^{-3} $M_\odot$ of first-peak r-process isotopes in a weak SN can explain the origin of the first-peak r-process isotopes in the Galaxy.

The smaller yield of the first-peak r-process isotopes from a single weak SN could be caused by differences in the progenitor structure. The main difference between a weak SN from a single star having a light CO core and an ultra-stripped SN is the possession of the He layer and the H-rich envelope. Because single stars have outer layers, part of the wind material would be decelerated by the outer layers and fall back onto the central region. In this case, the amount of ejected material would be reduced. Furthermore, the ejected wind material would be be subject to stronger neutrino irradiation to heat and eject accreting material. Strong neutrino irradiation increases the electron fraction of the wind material and thus prevents the

production of heavy elements. This process would also suppress heavy element production.

5 CONCLUSIONS

We have investigated the explosive nucleosynthesis of ultra-stripped Type Ic SNe for the CO145 and CO15 models. In weak SN explosions of $\sim 10^{50}$ erg, material with mass less than 0.1 $M_\odot$ having a shock-heated component and neutrino-irradiated ejecta is ejected. An ultra-stripped SN releases 0.006–0.01 $M_\odot$ of ^{56}Ni in our models. These SNe will be observed as fast-decaying Type Ic SNe with a peak magnitude of -15 to -16. The energy release by the radioactive decay of intermediate and heavy elements also contributes to the optical emission for several days after the explosion. The expected light-curves are less luminous than in the fast-decaying Type Ic SN 2005ek. If the explosion energy is higher and more ^{56}Ni is produced, ultra-stripped SNe could be more luminous. Ultra-stripped SNe are possible candidates for forming a class of binary neutron stars. Future observations of ultra-stripped Type Ib/Ic SNe will give a constraint on the merger rate for this class of binary neutron stars.

Light trans-iron elements are produced mainly in the neutrino-irradiated ejecta of ultra-stripped SNe. Although the elements of Ga–Zr are produced, their abundance distribution and total yield are not clearly determined because of the uncertainty in the electron fraction distribution of the neutrino-irradiated ejecta. The obtained yield of the first-peak r-process isotopes is less than 0.01 $M_\odot$, but it could be much smaller. The explosion of SNe evolved from single stars having a light CO core will also be weak, similar to the case for ultra-stripped SNe. Ultra-stripped SNe and weak SNe having a light CO core are possible production sites for light r-process isotopes during the chemical evolution of the Galaxy and in the Solar system. These SNe could also produce neutron-rich intermediate isotope ^{48}Ca.

ACKNOWLEDGEMENTS

We thank Shinya Wanajo, Ko Nakamura, Tomoya Takiwaki and Hans-Thomas Janka for valuable discussions. TY acknowledges the hospitality of the Yukawa Institute for Theoretical Physics (YITP) at Kyoto University during Yukawa International Program for Quark-Hadron Sciences (YIPQS) long term, and the Nishinomiya-Yukawa memorial workshop on 'Nuclear Physics, Compact Stars, and Compact Star Mergers 2016' (YITP-T-16-02). Numerical computations in this study were in part carried out on XC30 at Center for Computational Astrophysics in National Astronomical Observatory of Japan and on SR 16000 and XC40 at YITP at Kyoto University. KT was supported by research fellowships of Japan Society for the Promotion of Science (JSPS) for Young Scientists. This work was supported by the Grants-in-Aid for Scientific Research on Innovative Areas (Nos. 26104007, 16H00869) from the Ministry of Education, Culture, Sports, Science and Technology, the Grants-in-Aid for Scientific Research (Nos. 24244028, 26400220, 26400271, 16H02183, 16K17665) from JSPS, and Joint Institute for Computational Fundamental Science as a priority issue (Elucidation of the fundamental laws and evolution of the universe) to be tackled using Post 'K' Computer.

REFERENCES

Arnett W. D., 1982, ApJ, 253, 785
Asplund M., Grevesse N., Sauval A. J., Scott P., 2009, ARA&A, 47, 481
Buras R., Rampp M., Janka H.-Th., Kifonidis K., 2006, A&A, 447, 1049
Colgate S. A., Petschek A. G., Kriese J. T., 1980, ApJ, 237, L81
Colgate S. A., Fryer C. L., Hand K. P., 1997, in Ruiz-Lapuente P., Canal R., Isern J., eds, Thermonuclear Supernovae. Kluwer, Dordrecht, p. 273
Drout M. R. et al., 2013, ApJ, 774, 58
Drout M. R. et al., 2014, ApJ, 794, 23
Fischer T., Whitehouse S. C., Mezzacappa A., Thielemann F.-K., Liebendörfer M., 2010, A&A, 517, A80
Foley R. J. et al., 2013, ApJ, 767, 57
Fröhlich C. et al., 2006, ApJ, 637, 415
Fujibayashi S., Yoshida T., Sekiguchi Y., 2015, ApJ, 810, 115
Goriely S., Bauswein A., Just O., Pllumbi E., Janka H.-Th., 2015, MNRAS., 452, 3894
Hirai Y., Ishimaru Y., Saitoh T. R., Fujii M. S., Hidaka J., Kajino T., 2015, ApJ, 814, 41
Hoffman R. D., Woosley S. E., Fuller G. M., Meyer B. S., 1996, ApJ, 460, 478
Hotokezaka K., Kyutoku K., Tanaka M., Kiuchi K., Sekiguchi Y., Shibata M., Wanajo S., 2013, ApJ, 778, L16
Hotokezaka K., Piran T., Paul M., 2015, Nature Phys., 11, 1042
Ishimaru Y., Wanajo S., Prantzos N., 2015, ApJ, 804, L35
Janka H.-Th., Müller B., Kitaura F. S., Buras R., 2008, A&A, 485, 199
Just O., Bauswein A., Ardevol Pulpillo R., Goriely S., Janka H.-T., 2015, MNRAS, 448, 541
Komiya Y., Yamada S., Suda T., Fujimoto M. Y., 2014, ApJ, 783, 132
Lodders K., Palme H., Gail H.-P., 2009, in Trümper J. E., ed., Abundances of the Elements in the Solar System. In Landolt–Börnstein, New Series, Vol. VI/4B, Chap. 4.4. Springer-Verlag, Berlin Heidelberg
Meyer B. S., Krishnan T. D., Clayton D. D., 1996, ApJ, 462, 825
Meyer B. S., Krishnan T. D., Clayton D. D., 1998, ApJ, 498, 808
Moriya T. J. et al., 2017, MNRAS, 466, 2085
Müller B., 2016, PASA, 33, e048
Müller B., Janka H.-Th., Heger A., 2012, ApJ, 761, 72
Nadyozhin D. K., 1994, ApJS, 92, 527
Nomoto K., 1987, ApJ, 322, 206
Nomoto K., Hashimoto M., 1988, Phys. Rep., 163, 13
Podsiadlowski Ph., Dewi J. D. M., Lesaffre P., Miller J. C., Newton W. G., Stone J. R., 2005, MNRAS, 361, 1243
Pruet J., Woosley S. E., Buras R., Janka H. T., Hoffman R. D., 2005, ApJ, 623, 325
Sekiguchi Y., Kiuchi K., Kyutoku K., Shibata M., 2015, Phys. Rev. D, 91, 064059
Sekiguchi Y., Kiuchi K., Kyutoku K., Shibata M., Taniguchi K., 2016, Phys. Rev. D, 93, 124046
Shen S., Cooke R. J., Ramirez-Ruiz E., Madau P., Mayer L., Guedes J., 2015, ApJ, 807, 115
Sneden C., Cowan J. J., Gallino R., 2008, ARA&A, 46, 241
Suwa Y., Kotake K., Takiwaki T., Whitehouse S. C., Liebendörfer M., Sato K., 2010, PASJ, 62, L49
Suwa Y., Yoshida T., Shibata M., Umeda H., Takahashi K., 2015, MNRAS, 454, 3073
Tanaka M., Hotokezaka K., 2013 ApJ, 775, 113
Tanvir N. R., Levan A. J., Fruchter A. S., Hjorth J., Hounsell R. A., Wiersema K., Tunnicliffe R. L., 2013, Nature, 500, 547
Tauris T. M., Langer N., Moriya T. J., Podsiadlowski P., Yoon S.-C., Blinnikov S. I., 2013, ApJ, 778, L23
Tauris T. M., Langer N., Podsiadlowski P., 2015, MNRAS, 451, 2123
Tauris T. M. et al., 2017, ApJ, in press (arXiv:1706.09438)
Tsujimoto T., Shigeyama T., 2014a, A&A, 565, L5
Tsujimoto T., Shigeyama T., 2014b, ApJ, 795, L18
Umeda H., Yoshida T., Takahashi K., 2012, Progr. Theor. Exp. Phys., 01A302
van de Voort F., Quataert E., Hopkins P. F., Kereš D., Faucher-Giguère C.-A., 2015, MNRAS, 447, 140
Wanajo S., Janka H.-Th., Müller B., 2011, ApJ, 726, L15
Wanajo S., Janka H.-Th., Müller B., 2013a, ApJ, 767, L26
Wanajo S., Janka H.-Th., Müller B., 2013b, ApJ, 774, L6
Wanajo S., Sekiguchi Y., Nishimura N., Kiuchi K., Kyutoku K., Shibata M., 2014, ApJ, 789, L39

Wanajo S., Müller B., Janka H.-Th., Heger A., 2017, ApJ, preprint (arXiv:1701.06786)
Woosley S. E., 1997, ApJ, 476, 801
Woosley S. E., Heager A., 2015, ApJ, 810, 34
Woosley S. E., Weaver T. A., Taam R. E., 1980, in Wheeler J.C., ed., Proc. Texas Workshop on Type I Supernovae. Univ. Texas, Austin, p. 96
Woosley S. E., Hartmann D. H., Hoffman R. D., Haxton W. C., 1990, ApJ, 356, 272
Yoshida T., Umeda H., Nomoto K., 2008, ApJ, 672, 1043
Yoshida T., Takahashi K., Umeda H., Ishidoshiro K., 2016, Phys. Rev. D, 93, 123012

APPENDIX A: ELECTRON-CAPTURE SN YIELD

In order to discern the systematic differences among explosion models, we performed a two-dimensional numerical simulation for the explosion of an ECSN using our radiation-hydrodynamics code. The ECSN progenitor was adopted from a 1.3776 $M_\odot$ O-Ne-Mg core evolved from an 8.8 $M_\odot$ star (Nomoto 1987). The simulation method for the SN is the same as the explosion simulation for the ultra-stripped SNe in this study. We pursued the explosion for 667 ms after the core bounce. We obtained an ejecta mass of 5.4×10^{-2} $M_\odot$ and an explosion energy of 3.2×10^{50} erg.

We then calculated the explosive nucleosynthesis of the ECSN ejecta using 13 331 tracer fluid particles having a positive energy and positive radial velocity. Fig. A1 shows the ejected mass in each bin of Y_e at the initial time of the nucleosynthesis calculation. The minimum Y_e value of the ECSN ejecta is 0.288, which is smaller than the corresponding values found in Wanajo et al. (2011) and Janka (2016, private communication; see Section 4.2). We also see a peak of the ejected mass in the range between $Y_e = 0.35$ and 0.40. We do not see a peak in the lowest Y_e component. In the ultra-stripped SN models, the duration between collapse and shock launch is longer than in the ECSN model. Because the shock launch takes place later, some material stays above PNS for a while. Once the shock is launched, the long-staying material is ejected together with material just captured by the shock. These two components produce the low-Y_e peak in the ultra-stripped SN models.

In our ECSN model, the mass of ^{56}Ni ejected is 1.1×10^{-3} $M_\odot$. This is smaller than the corresponding mass found in Wanajo et al. (2011) by a factor of 3. The elemental abundance ratio of the ECSN ejecta to the solar abundance is shown in Fig. A2. In this model, the elements between As and Cd have high abundance ratios. The ECSN model produces heavier elements than the ultra-stripped SNe. This is owing to the ejection of more neutron-rich material compared with the ejecta of the ultra-stripped SNe. In this calculation, elements heavier than Mo are produced only in the ejecta of $Y_e \lesssim 0.37$. The mass of light trans-iron elements in the ECSN ejecta is 3.3×10^{-2} $M_\odot$. This large yield is also due to the ejection of the neutron-rich material. This model also produces heavier elements than the ECSN model in Wanajo et al. (2011). The abundance distribution of the heavy elements is roughly consistent with their model with $Y_{e,min} = 0.30$.

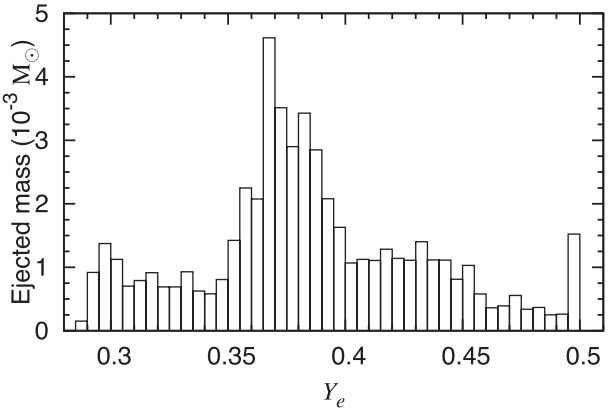

Figure A1. The ejected mass in each bin of Y_e at the initial time of the nucleosynthesis calculation of the ECSN model. The vertical axis indicates the ejected mass in units of 10^{-3} $M_\odot$ within each Y_e bin in the range of $\Delta Y_e = 0.005$.

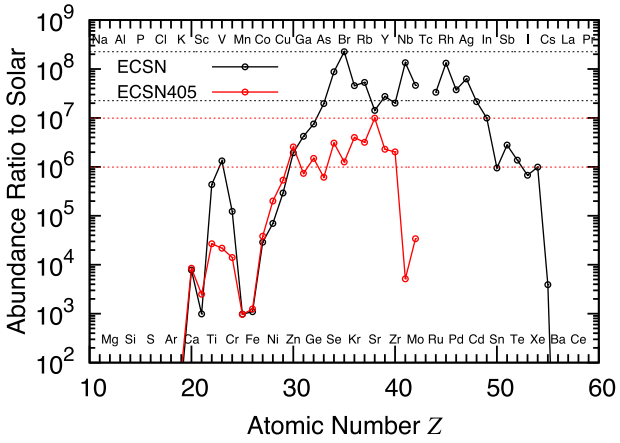

Figure A2. Elemental abundance ratios in the ejecta of the ECSN to the solar abundance. The black and red lines denote the ratios of the ECSN model and the modified Y_e ECSN (ECSN405) model, respectively. The dashed lines denote the maximum ratios and the ratios of the 10 per cent of the maximum ratios.

In order to investigate differences in the abundance distribution resulting from the Y_e distribution, we also calculated the explosive nucleosynthesis, changing the Y_e distribution in accordance with equation (1) and $Y_{e,min} = 0.405$, which is close to the minimum of the ECSN model in Wanajo et al. (2011). We denote this model as ECSN405. This model produces a ^{56}Ni yield of 1.36×10^{-3} $M_\odot$. The elemental abundance ratio of the ECSN405 model to the solar abundance is also shown in Fig. A2. The light trans-iron elements between Ge and Zr have high abundance ratios. However, elements heavier than Zr are not produced in this model. The distribution of the abundance ratio is consistent with the ECSN model in Wanajo et al. (2011). The total yield of the heavy elements in this model is 3.6×10^{-3} $M_\odot$. This yield is smaller than that of the original model by a factor of 9, so the total yield also depends on the Y_e distribution.

In the case of the ECSN, our explosion model indicates a larger ejecta mass, a higher explosion energy, and the ejection of more neutron-rich material compared with the explosion model in Wanajo et al. (2011) (see also Janka et al. 2008). These differences could be due to the different treatments of neutrino transport. The differences found in the SN ejecta would influence the explosive nucleosynthesis. As a result, a larger yield of heavy elements, including elements heavier than light trans-iron elements up to Cd, is produced in our model. When we change the Y_e distribution to shift the minimum Y_e value to 0.405, the heavy elements produced are Ga–Zr. So, our model produces more neutron-rich material than the models in Janka et al. (2008), which is preferable to producing heavier r-elements. Note that the above uncertainties are also included in the

ultra-stripped SN models and these uncertainties would also affect the abundance distributions of ultra-stripped SNe.

APPENDIX B: ISOTOPIC ABUNDANCE RATIOS IN MODIFIED ELECTRON-FRACTION CASES FOR THE CO145 MODEL

The isotopic abundance ratios to the Solar system composition in the Ye-W and Ye-B models are shown in Fig. B1. We see in the Ye-W model that neutron-rich isotopes are produced in $Z < 30$ elements and neutron-deficient ones are produced in $Z \geq 30$ elements. A high abundance ratio is obtained for the neutron-rich isotope ^{48}Ca. Heavy-element isotopes ^{90}Zr and ^{92}Mo are also produced. In the Ye-B model, the neutron-deficient heavy isotopes ^{74}Se and ^{78}Kr are produced. They are produced mainly in the most neutron-rich material ($Y_e \sim 0.47$–0.48).

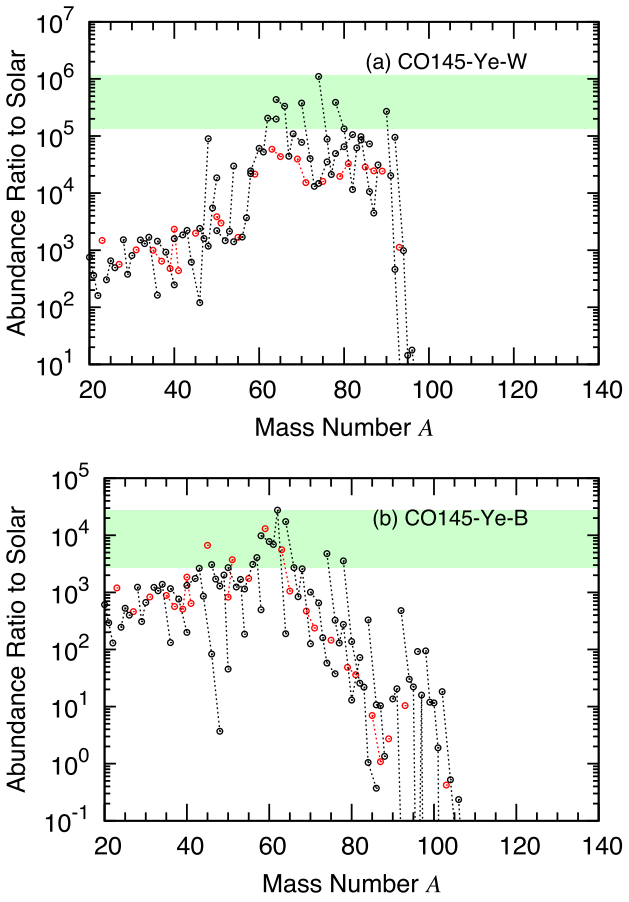

Figure B1. As Fig. 5, but for the (a) CO145-Ye-W and (b) CO145-Ye-B models.

This paper has been typeset from a TEX/LATEX file prepared by the author.